ELSEVIER

Contents lists available at ScienceDirect

Journal of Alloys and Compounds

journal homepage: www.elsevier.com/locate/jalcom



Helical spin ordering in room-temperature metallic antiferromagnet Fe_3Ga_4



Brandon Wilfong^a, Adrian Fedorko^b, Danil R. Baigutlin^{c,d}, Olga N. Miroshkina^{c,e}, Xiuquan Zhou^f, Gregory M. Stephen^g, Adam L. Friedman^g, Vaibhav Sharma^h, Omar Bishop^h, Radhika Barua^h, Steven P. Bennettⁱ, Duck Young Chung^f, Mercouri G. Kanatzidis^{f,j}, Vasiliy D. Buchelnikov^c, Vladimir V. Sokolovskiy^c, Bernardo Barbiellini^{d,b}, Arun Bansil^b, Don Heiman^{b,k}, Michelle E. Jamer^{a,*}

- ^a Physics Department, United States Naval Academy, Annapolis, MD 20899, USA
- ^b Physics Department, Northeastern University, Boston, MA 02115, USA
- ^c Faculty of Physics, Chelyabinsk State University, 454001Chelyabinsk, Russia
- ^d Department of Physics, School of Engineering Science, LUT University, FI-53850 Lappeenranta, Finland
- e Department of Physics and Center for Nanointegration, CENIDE, University of Duisburg-Essen, 47048 Duisburg, Germany
- f Materials Science Division, Argonne National Laboratory, 9700 South Cass Avenue, Lemont, IL 60439, USA
- g Laboratory for Physical Sciences, College Park, MD 20740, USA
- ^h Mechanical and Nuclear Engineering, Virginia Commonwealth University, Richmond, VA 23220, USA
- ⁱ Material Science and Technology Division, US Naval Research Laboratory, Washington, DC 20375, USA
- ^j Department of Chemistry, Northwestern University, Evanston, IL 60208, USA
- ^k Plasma Science and Fusion Center, MIT, Cambridge, MA 02139, USA

ARTICLE INFO

Article history: Received 12 January 2022 Received in revised form 9 May 2022 Accepted 17 May 2022 Available online 20 May 2022

Keywords:
Magnetically ordered materials
Transition metal alloy and compounds
Metamagnetism
Growth from vapor
Density functional theory (DFT)

ABSTRACT

Metallic Fe₃Ga₄ displays a complex magnetic phase diagram that supports an intermediate antiferromagnetic (AFM) helical spin structure (HSS) state at room temperature which lies between two ferromagnetic (FM) phases. Magnetic measurements along the three crystallographic axes were performed in order to develop a model for the temperature and field dependence of the HSS state. These results show that the AFM state is a helically ordered spiral propagating along the *c*-axis with the magnetic moments rotating in the *ab*-plane. Under applied magnetic field, the AFM state exhibits a metamagnetic transition to conical ordering before entering a fully field-polarized FM state at high fields. The conical ordering in the AFM state is anisotropic even within the *ab*-plane and may gives rise to Berry phase effects in transport measurements. Metallic conductivity from density of states computations was confirmed through resistivity measurements and no anomalous behavior was observed through the various magnetic transitions. Published by Elsevier B.V.

1. Introduction

Antiferromagnetic (AFM) materials have been at the forefront of materials research in recent years due to their potential use in spintronics applications [1,2]. In particular, materials which combine room-temperature metallic and AFM behaviors offer an excellent platform for fundamental exploration as well as device and memory applications usage due to the interplay of charge and spin transport [3]. The competition between itinerant and local moments drives exotic physical phenomena that can give rise to the formation of

* Corresponding author. E-mail address: jamer@usna.edu (M.E. Jamer). metallic helically-ordered AFM states, which were studied extensively in simple intermetallic systems [4,5].

The relevance of AFM materials for spintronics applications is due to their femtosecond response times for high-frequency electronics and the lack of fringing fields in high-density devices [1,6]. There are also advantages in the ability to vary the magnetism with external controls of thermal, magnetic, electrical or strain fields. FeRh is a classic material having an abrupt transition between the AFM and ferromagnetic (FM) phases that can be varied by temperature [7], magnetic field [8], alloying [9], or strain [10,11]. There is great need to enlarge the palette of such materials for the exploration of fundamental properties as well as for developing next-generation spin-related devices.

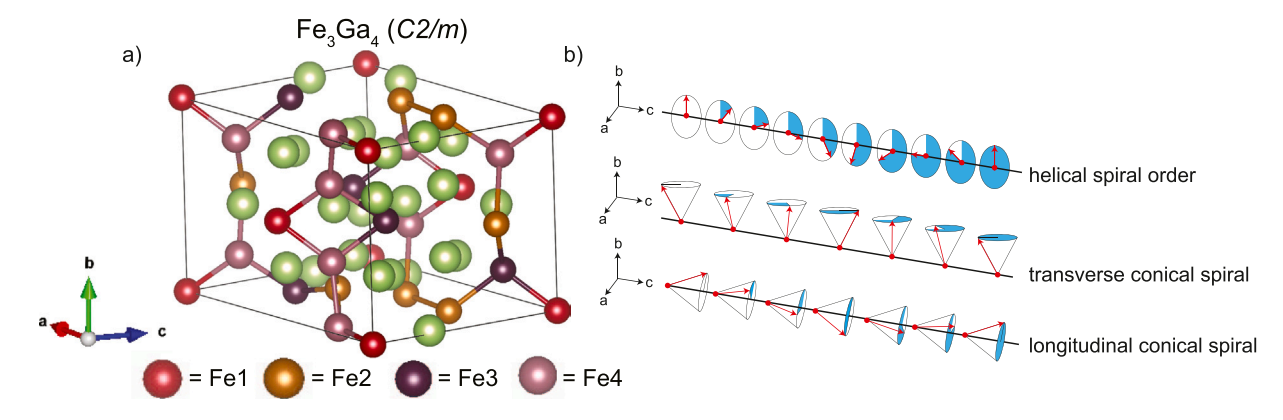


Fig. 1. (a) Crystal structure of Fe₃Ga₄ shown with stacked Fe layers along the b-axis. Inequivalent Fe atoms are shown in different colors while all Ga atoms are displayed as green atoms. Relevant inter- and intra-layer Fe-Fe distances which are less than 3 Å are shown. (b) Representative schematics of the evolution of ab-plane helical order to the observed metamagnetic phases at higher applied fields within the intermediate AFM helical spin phase.

To that end, a material of interest is the intermetallic Fe₃Ga₄, which exhibits a complex magnetic phase diagram along with a metallic ground state [12]. This complex magnetic behavior originates from the interplay of itinerant and localized electrons and competing magnetic interactions in the Fe₃Ga₄ unit cell, Fig. 1. Initial work identified an intermediate AFM phase that exists over a wide temperature range (\sim 70–360 K) between a FM ground state (FM₁) and a high temperature FM phase (FM₂). In contrast to FeRh, recent work on Fe₃Ga₄ has determined that this intermediate AFM phase is a helical spin structure (HSS) and concluded that the FM ordering at low and high temperatures is likely the same state indicating that the helical ordering of the spins is in close competition to the FM ground state [13,14]. Here, we use HSS to describe the AFM phase instead of spin density wave (SDW) that was used in earlier literature. Neutron diffraction work found the AFM phase to be a spin spiral and suggested that the ground-state has amplitude-modulated helical ordering with the spins polarized along the a-axis [13]. However, theoretical work suggested that the helical phase has spins ordered with fixed amplitude in the ab-plane, in agreement with our experimental results. Finally, this HSS state could give rise to the observed topological Hall effect (THE) [12,15].

The three existing spin configurations in the AFM state which depend on field orientation and strength are illustrated in Fig. 1. The spins at low magnetic fields are configured helically and propagate along the c-axis with a \mathbf{q} -vector of (0, 0, 0.29), as determined from neutron diffraction. [13] Two other spin states are identified as shown: the transverse conical spiral (TCS) state and the longitudinal conical spiral (LCS) state. Spin orientations of the Fe moments in the helical state were determined from measurements of the magnetization carried out with fields applied along the crystal axes as a function of temperature. The spin orientation at zero field is a helical spin spiral propagating along the c-axis with moments rotating in the *ab*-plane. Applying a magnetic field transforms the intermediate state into the transverse and longitudinal conical spiral configurations described above depending on field strength and orientation. The AFM state is metallic as revealed by the high spin-density of states at the Fermi energy in first-principles computations, and verified by metallic behavior in the temperature-dependent resistivity. This work aims to deepen the understanding of the magnetic ordering in Fe₃Ga₄ in both the FM states as well as the intermediate AFM phase and resolve the outstanding issues related to the understanding of metamagnetic ordering of the HSS.

2. Experimental and computational details

Single crystals of Fe₃Ga₄ were synthesized using a chemical vapor transport (CVT) method adapted from previous work. [16]

Elemental Fe granules (Alfa Aesar 99.98%) and Ga solid (Alfa Aesar 99.99%) were added in a molar ratio of Fe:Ga (68:32) to a quartz tube along with I_2 chips (Alfa Aesar 99.5%) in a concentration of 18×10^{-6} moles/cm³ based on the approximated volume of the sealed quartz tube. The elements inside the quartz tube were then evacuated to $< 7 \times 10^{-3}$ Torr and sealed. The quartz tube was arranged in a triple-zone furnace with the charge situated in the hot-end set to 700 °C and such that the cold-end was set to 650 °C in the remaining furnace zones. The growth was held at these temperature settings for four weeks before the furnace was turned off and allowed to cool to room temperature naturally. Long needle-like single crystals (approximately 0.5 mm wide and 0.25 mm thick with variable lengths up to 2 cm) were recovered from the cold-end of the quartz tube and washed with methanol. Single crystal X-ray diffraction data of Fe₃Ga₄ was obtained using a STOE IPDS diffractometer with Mo- $K\alpha$ radiation. The crystals generally had a long direction that was found to be the b-axis, and usually had several flat faces perpendicular to that long axis. The angles between the faces were measured optically and indicated that the faces were a (10-1) major plane and a (20-1) minor plane.

Magnetization measurements at ambient pressure were performed using a Quantum Design MPMS XL-7 SQUID (Superconducting Quantum Interference Device) magnetometer at various fields. For magnetization versus temperature [M(T)] scans, the crystal was first ZFC (zero-field cooled) to 10 K. A constant magnetic field was then applied along the appropriate crystallographic direction, and data was collected as the temperature was increased to 400 K. For magnetization versus applied field [M(H)]scans, the crystal was first ZFC to the desired temperature. The moment was then saturated, and data was collected for decreasing field. Resistivity measurements were performed in a closed-cycle variable-temperature cryostat set between the poles of a resistive magnet. Standard lock-in techniques were used with an applied current of 1 mA at 13 Hz. Field-cooling measurements were performed by heating the sample to 500 K and cooling under an applied field of 0.4 T.

The calculations were performed within the framework of the density functional theory (DFT) using the projector augmented-wave (PAW) method as implemented in the Vienna *Ab initio* Simulation Package (VASP) [17,18]. The generalized gradient approximation (GGA) [19] with Perdew-Burke-Ernzerhof (PBE) formulation was used for treating exchange-correlation effects. The following valence electron configurations in the PAW potentials were chosen: $(3p^64s^23d^6)$ for Fe and $(3d^{10}4s^24p^1)$ for Ga. The plane wave cut-off energy was 600 eV. The k-points in the reciprocal space were generated using the Monkhorst-Pack scheme[20]. The grid density of $\approx 1000 \ k$ -points in the Brillouin zone was used in the relaxation

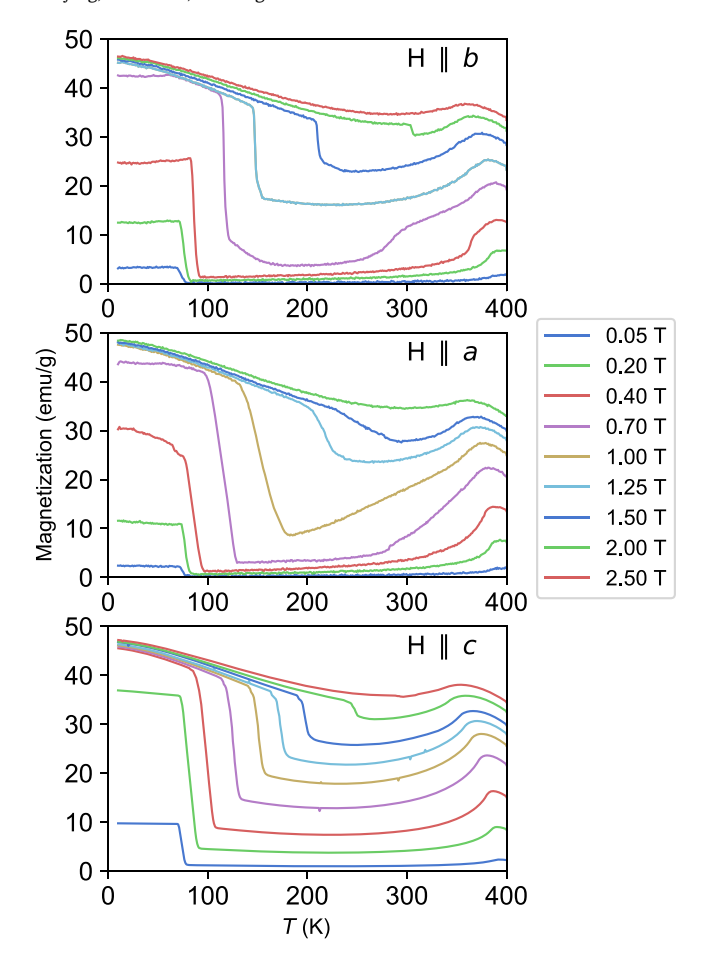


Fig. 2. Magnetization of Fe_3Ga_4 for the field applied along the three crystalline axes as a function of temperature and magnetic field. M(T) measured for field aligned along the [010] b-axis, [100] a-axis and [001] c-axis. The helically ordered AFM phase is seen at intermediate T, bracketed on either side by the FM phases. The sample was ZFC-cooled and M(T) was collected for increasing field.

procedure. Spin spiral calculations were performed using the generalized Bloch theorem formalism [21], therefore, spin-orbit coupling has not been included.

3. Results and discussion

3.1. Anisotropic single crystal magnetic properties

Magnetization of the oriented Fe_3Ga_4 crystals was measured in order to investigate the intermediate AFM and FM phases. Fig. 2 shows the total magnetization varying as a function of temperature and field for all three field directions relative to the monoclinic unit cell axes. Note that the moment is a strong function of both temperature and magnetic field for all three directions of the field. Figs. 2 shows complex evolution of M(T), similar to previous works, but in greater detail. [12,22–24,13] An intermediate low-moment helically ordered AFM phase lies between two FM-like phases over a very wide temperature range from approximately 70 to 360 K. The same general behavior is observed for all three crystallographic directions. We also observe that within the low-temperature FM₁ state the magnetization along the c-axis is much larger (3x at fields below 1T) compared to the a- and b-axes, indicating the easy c-axis at low fields.

Fig. 2 shows that the HSS phase can be suppressed at sufficiently high field and the FM₁ transition temperature increases rapidly for increasing field, increasing by more than 200 K at 2 T applied field. The FM₂ transition onset does not show as drastic of a change at high fields compared to the lower temperature transition, but the FM₂ transition does broaden at high fields before becoming not observable upon suppression of the intermediate AFM phase. The evolution of the intermediate phase to the field-polarized FM state is shown in these temperature-dependent magnetization measurements. Nonetheless, how the spins transition to the field-polarized FM state is not clear without isothermal magnetization. Fig. 3 thus illustrates how the M(H) transitions change for the three crystallographic directions. Data is shown for four temperatures: T = 30 K in the FM₁ phase; and 140, 210 and 280 K in the low-moment phase. In Fig. 3, for T = 30 K, the sample is fully in the FM₁ phase. The M(H)curves for the field along the b- and c-axis show mostly smooth saturating behavior. In particular, the b-axis is strictly linear until saturation - this is characteristic of the field canting the moment into the *b*-direction. We observe that the magnitude of magnetization in the FM state (below ~ 70 K) at low fields is much higher for field applied parallel to the c-axis than with field parallel to the a or baxis, indicating that the FM state is polarized in the c-direction, in direct agreement with previous results.[13] It is noted that the magnetization goes to zero with zero applied field.

The similarity of the low-field isothermal magnetization along the *a*- and *b*-axes provides support for an *ab*-plane helical order. Full analyses for the propagation vector requires the requires the use of neutron diffraction [25,26]. Additionally, isothermal magnetization measurements in the intermediate phase reveal a complex evolution of metamagnetic phases that are temperature, field and orientation dependent. These measurements support the helically ordered phase transitions in this compound.

3.2. Metamagnetism and spin configurations

More detailed investigation of the anisotropic field evolution of the magnetic properties reveals complex metamagnetic behavior of the ab-plane helical ordering. At temperatures of 140, 210, and 280 K, Fe₃Ga₄ is in the HSS phase at low fields and switches to a field-polarized FM phase at the highest measured fields, shown in Fig. 3. For fields below 0.7 T, the M(H) slopes for the a- and b-axes are almost identical, indicating isotropic behavior in this low-field regime. In contrast, the slope for the c-axis is much larger and linear over the wide field region within the HSS phase, which is assigned to canting of spins in the *ab*-plane toward the *c*-axis. For fields applied along the c-axis, we observe a linear increase in magnetization before a spin-flop into a field-polarized FM state at a critical field (H_c) which increases with increasing temperature. In Fe₃Ga₄, the T =0 ground state is FM, and we see that as the temperature approaches the FM₁ transition, H_c will be suppressed as saturation occurs at lower field. Through these observations, we can determine that within the HSS phase the c-axis is the easy axis. The easy axis behavior of the c-axis even within the HSS state is likely due to the proximity of the c-axis polarized FM state within the energy land-

The evolution of the response to field applied in the *ab*-plane in the HSS is more complex and the key differences in the in-helical-plane anisotropy within the system can be observed only at higher applied fields. At low fields, both show qualitatively similar behavior which is to be expected for *ab*-plane helical order, but not for an *a*-axis amplitude modulated HSS as suggested in earlier work [13]. Previous work catalogued the combined behavior of the *ab*-plane; however, our work shows the anisotropy between the *a*- and *b*-axis

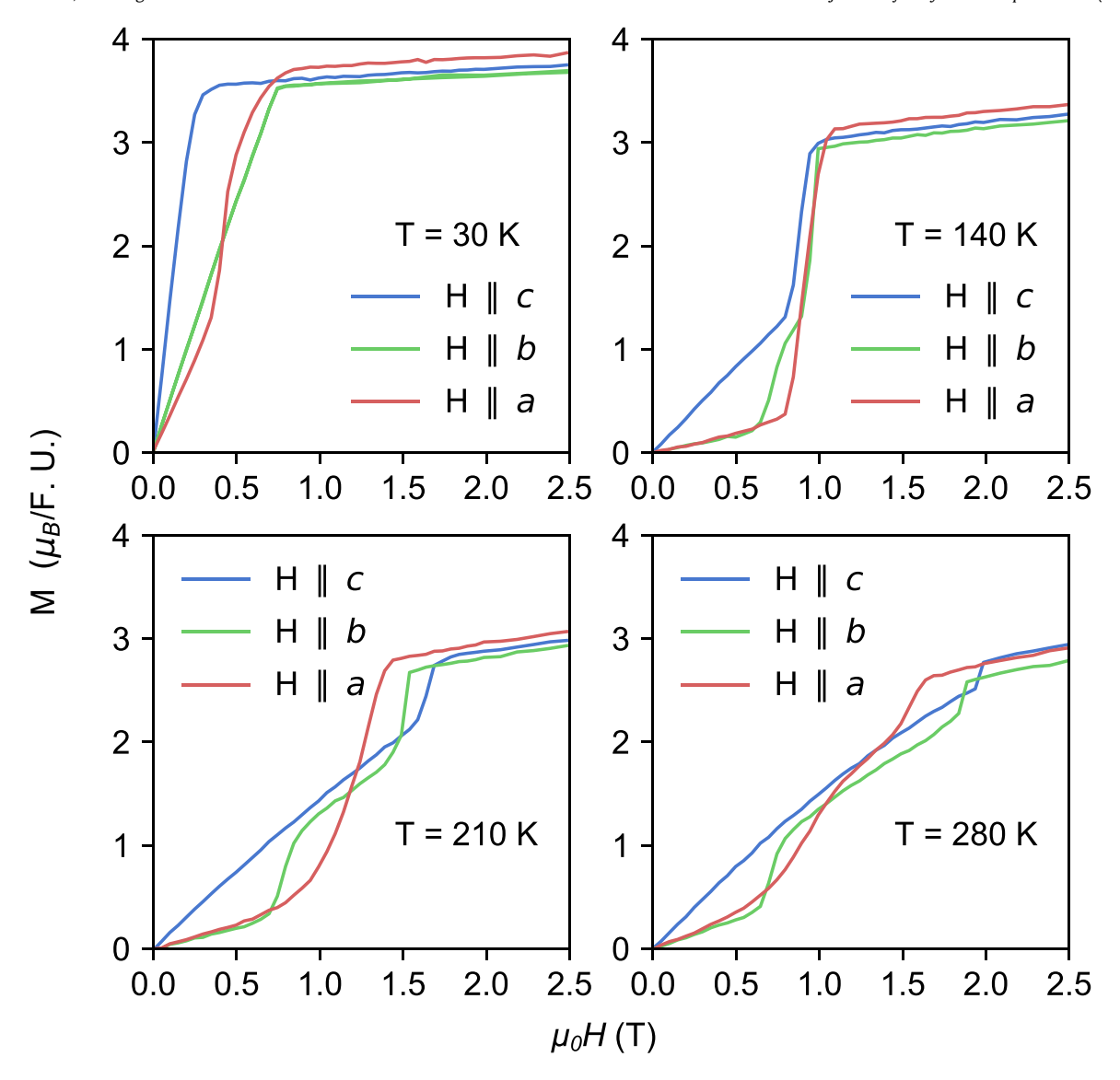


Fig. 3. Magnetization of Fe_3Ga_4 for fields applied along the three crystallographic directions at various temperatures. The helical spin state dominates at fields below H = 0.7 T at the higher temperatures T = 140, 210, and 280 K.

behavior is significant [12]. For all temperatures, applied field along the b-axis creates two observable metamagnetic transitions, whereas the a-axis yields one metamagnetic transition except for the 280 K isotherm. In all cases, at the highest field, a field-polarized FM state is found. For field applied parallel to the *b*-axis we observe an initial metamagnetic transition at approximately the same field $(H = 0.75 \,\mathrm{T})$ for all temperatures shown followed by an additional metamagnetic transition to the field-polarized FM state that ranges from 1 T at 140 K to 1.75 T at 280 K. The field-range stability of the intermediate phase increases linearly with temperature. In comparison, field applied parallel to the a-axis shows one metamagnetic transition, which increases from 0.9 T at 140 K to 1.2 T at 210 K to the field-polarized FM state. At 280 K, we reveal two metamagnetic transitions similar to the behavior observed for field parallel to the b-axis, but the low-field transition is much broader. Since the HSS state is an ab-plane helical order, it is unclear why there is significant anisotropy between the behavior of the a - and b-axes at higher applied fields. Without temperature and field-dependent neutron diffraction we cannot assign the exact nature of field-induced

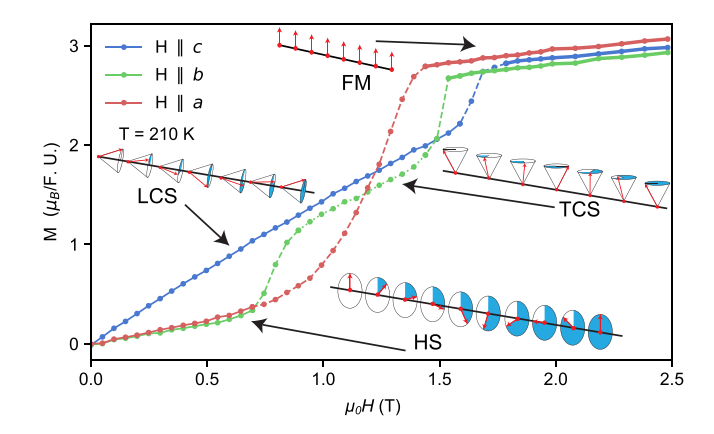


Fig. 4. Magnetic moment as a function of field applied along the crystalline axes at $T = 210 \, \text{K}$. Different line styles represent regions of different metamagnetic ordering. Illustration of the various spin configurations that evolve as a function of field for the helical spin (HS), transverse conical spin (TCS), and longitudinal conical spin (LCS) states.

metamagnetic phases as the field-polarized FM phase approached. However, we can discuss them qualitatively as the behavior of the HSS phase does appear to be similar to the in-helical-plane behavior of YMn_6Sn_6 , which has been shown to be related to Fe_3Ga_4 in recent works [15,27].

The qualitative interpretation of the magnetic field evolution of the HSS is summarized in Fig. 4. For fields applied along the a – and b-axes, the low-field M(H) slopes are almost identical for fields below 0.7 T as the spins rotate in the ab-plane, but the screw-like helix is biased toward a configuration that is offset from the c-axis toward the field direction. There is a rapid increase in moment above 0.7 T for the *b*-axis that is consistent with a spin-flop-like transition into a TCS state at higher fields [27,28]. Recent theoretical and experimental work has found that this TCS state can generate a nonzero topological field in the presence of an external applied field, which likely explains the observed THE[15,12,27]. The moment increase above 1.5 T for 210 K results from the transition of the HSS to the field-polarized FM state. For all data, when the field is applied parallel to the c-axis, (the propagation direction of the spin spiral order) we see a linear increase in magnetization due to the formation of a LCS as the spins are canted out of helical ab-plane until a field-polarized FM state is recovered above 1.7 T applied field. The correct assignment of the metamagnetic phases in the HSS regime would require further investigation.

To summarize, the anisotropic magnetization measurements performed in this work support the identification of the HSS phase as a *ab*-plane helical phase where the ordering propagates along the *c*-axis [15]. Although a different magnetic ordering solution was found in the earlier work, the previous classification of this phase using neutron diffraction could not rule out this ordering type due to the use of unpolarized neutron diffraction [13]. Additionally, our experimental work qualitatively confirms the expected metamagnetic behavior associated with an *ab*-plane helical state that can be paired with theoretical results.[12,27]. Further experimental investigation is required to determine the details of the magnetic ordering in the HSS phase as well as to determine the mechanism for the formation of the HSS phase between the high- and low-temperature FM phases.

3.3. Ground state energies

To explain the intermediate AFM phase helical order, we have performed DFT calculations to determine the magnetic ground state of the system. Correlation effects beyond GGA are almost absent since the Hubbard repulsion parameter U is close to the Hund's rule coupling Ji in this system [15]. Therefore, treating the exchange-correlation effects within GGA is sufficient for studying the ground state of Fe₃Ga₄ and for calculating the energy difference between the FM and AFM states. DFT-nased analysis of Afshar $et\ al.\ [15]$ has previously predicted the ground state to be a helically-ordered spin spiral propagating along the c-axis with spins rotating within the ab-plane. Our results presented in Table 1 show that a c-axis ordered FM

Table 1 Energy difference (ΔE) between the FM, HSS magnetic states with $\mathbf{q} = (0, 0, 0.25)$, and the two different collinear AFM states with illustrated spin configurations. The energy of FM state is taken to be zero.

Magnetic state	V (Å ³)	μ_{tot} , ($\mu_B/\text{f.u.}$)	ΔE , (meV/atom)
HSS q=(0,0,0.25)	578.109	5.430	-0.994
FM	579.070	5.869	0
AFM ₁	577.677	0	27.69
AFM ₂	584.189	0	326.84

state is extremely close in energy to the helical phase with propagation vector $\mathbf{q} = (0, 0, 0.25)$ (see Supplemental Information (SI), Figure S1). Our calculations show that the HSS-AFM is energetically favorable in comparison to the experimentally observed FM ground state. The energy difference between the two states corresponds to a temperature difference of approximately 11.6 K, which is slightly less than the FM₁ transition temperature observed in our experiments. We expect that inclusion of finite temperature contributions to free energies of both the phases will yield a higher transition temperature closer to $\approx 70\,\mathrm{K}$. However, free energy calculations are beyond the scope of the present study.

The total magnetic moment increases upon the transition between HS-AFM and FM state, because the magnetic moments of individual Fe atoms become collinear with respect to each other, and we observe that the unit cell volume decreases through this transition. The calculated moments are listed in Table 1 and are larger for both states than the corresponding saturation magnetization in the HSS-AFM and FM states observed in the experiment. Notice that the simulation of the FM state yields similar sized magnetic moments with an average of 2.02 μ_B /Fe, with moments ranging from 1.82 to 2.24 μ_B /Fe in line with other calculations [12]. However, comparison with experiment shows the slight difference with Fe moment size of ~ 1.25 μ_B at saturation in the FM state likely due to additional itinerant nature of the Fe electrons in this system.

Other collinear AFM ordered states are much higher in energy compared to the c-axis ordered FM state (see SI, Figure S1). The estimated transition temperature of $\approx 320\,\mathrm{K}$ between the most energetically favorable AFM $_1$ and FM phaseis more than the experimental value of $\approx 70\,\mathrm{K}$. In line with the finding of Afshar et al. [15] we were also not able to stabilize the amplitude-modulated HSS phase reported by Wu et al. [13,15] The helical spin spiral state with propagation vector $\mathbf{q} = (0, 0, 0.25)$ and the associated magnetic unit cell is depicted in SI Figure S2, which shows how the magnetic moments in the ab-plane change along the c-axis propagation and vary between the unique Fe sites in the lattice. Further neutron diffraction work is needed to systemically determine helical spin spiral order and the corresponding Fe-site magnetic moments to determine how Fe-Fe interactions affect the magnetic order.

Fig. 5 shows the Fermi surface of Fe $_3$ Ga $_4$ in the FM state and the contributions from different electronic bands. The nesting appears only for the Fermi sheet # 312 along the direction of spin spiral vector Γ - Z observed experimentally. This can also follow from Fig. 5(a), which depicts the generalized susceptibility of each band along the Γ - Z direction. The intraband transition # 312 has a smooth maximum at $\mathbf{q} \approx (0, 0, 0.22)$, however when the contribution of all sheets is taken into account, the peak in generalized susceptibility has disappeared. Thus, most likely, the nesting of the Fermi surface is not responsible for the transition to the AFM-type state. These results are consistent with the work of Mazin *et al.* and emphasize the need for additional characterization to determine the mechanism for the stabilization of the intermediate helically ordered state [15].

3.4. Metallicity and electronic properties

Electrical resistivity measurements confirm the metallic nature of our Fe $_3$ Ga $_4$ crystals. Fig. 6 shows that the resistivity $\rho(T)$ increases with temperature, over the entire temperature range in line with Refs. [12,13], who report anomalous behavior in the range of the HSS-FM $_2$ transition, which could be evidence of the electronic nature of the HSS instability in this system. However, we have not observed any anomalous behavior in this regime. This is significant because

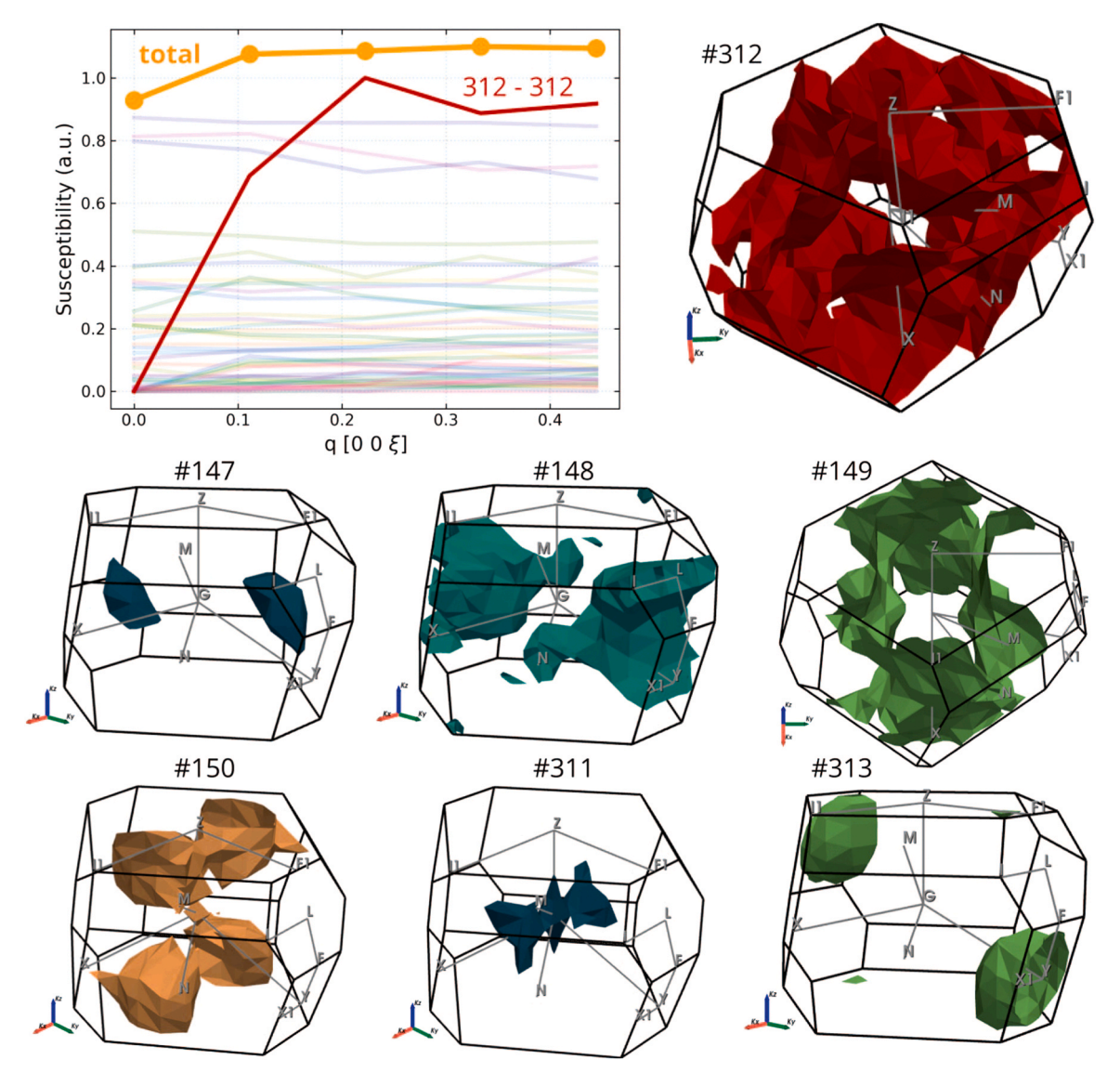


Fig. 5. Fermi surfaces associated with different bands and the generalized electronic susceptibility for FM state of Fe₃Ga₄.

previous work discussed this proposed anomalous behavior in the context of illustrating the change in electronic behavior due to HSS ordering. It must be noted that we did measure small jumps in resistivity at random temperatures, consistent with telegraph noise from contact effects, such as oxidation [29,30]. However, we did not observe a jump at a consistent temperature as reported previously [13] In light of not observing this behavior in our data, the lack of observed anomalous behavior in the original characterization of Fe_3Ga_4 single crystals [12], and the lack of \mathbf{q} -dependent maximum in the generalized susceptibility at the Fermi surface, we propose the mechanism for the formation of the HSS in this system is likely not solely driven by electronic factors. The magnetic transitions here might be ascribed to a competition between the nearly degenerate magnetic states arising from the combination of localized and itinerant electrons and the complex Fe-Fe interactions.

Resistivity measurements also reveal a deviation from expected linear temperature dependence below 200 K and an inflection point in the temperature derivative of resistivity at the FM₁-HSS transition, see inset of Fig. 6. One can see a broad peak in the derivative of resistivity with respect to temperature that has a maximum at the FM₁-HSS transition. This change in scaling behavior is indicative of additional scattering due the magnetic ordering in this regime.

Density of states calculations performed for the FM state and the HSS state confirm the metallic behavior of ${\rm Fe_3Ga_4}$ as seen in Fig. 7. Within the HSS state, a small shift in spectral weight at the Fermi level is observable and is identified as a pseudo-gap effect toward higher energies [15]. These calculations support the identification of the magnetic order of the intermediate HSS as a helical spin spiral ordered phase as opposed to the previously reported amplitude modulated phase. However, in order to accurately determine the

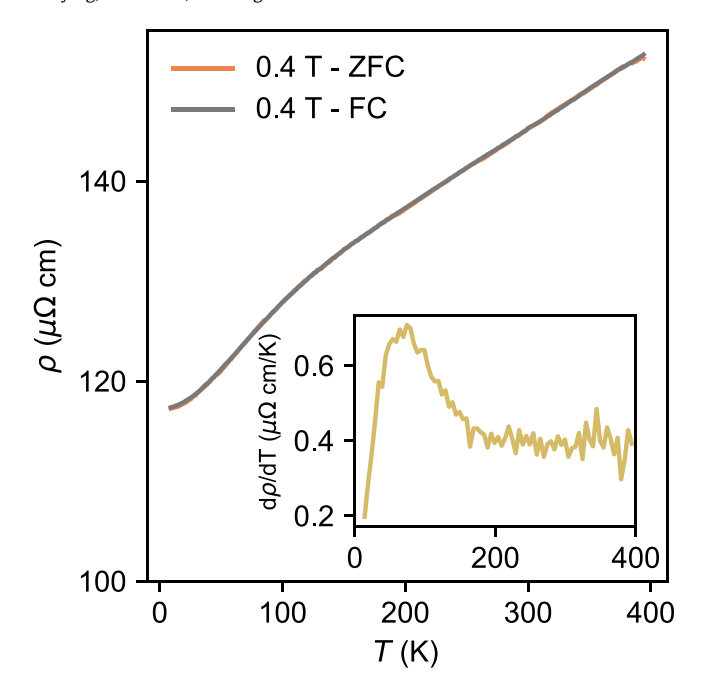


Fig. 6. Temperature-dependent resistivity of Fe_3Ga_4 measured upon heating and cooling in an external field of 0.04 T. Inset shows the derivative of resistivity with respect to temperature and emphasizes the deviation from linearity below 200 K.

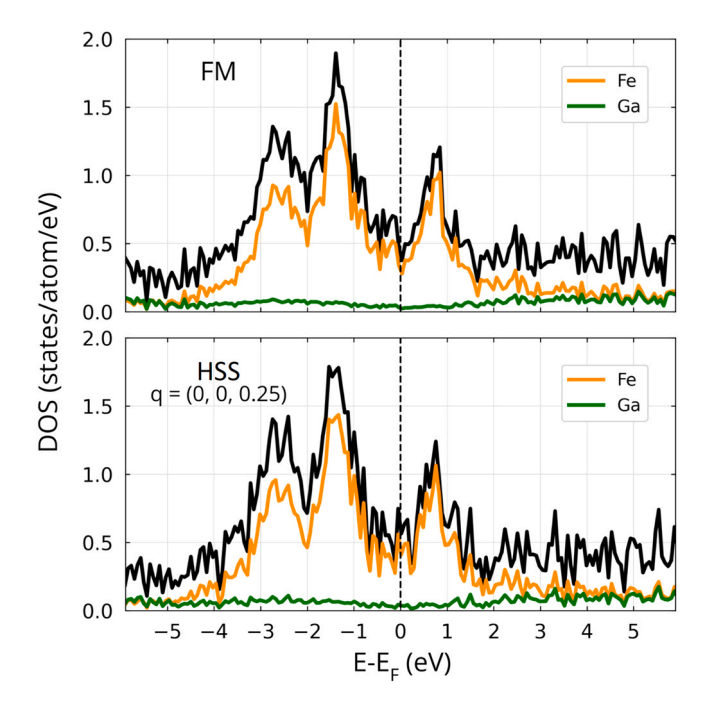


Fig. 7. Theoretical density of states calculations are shown for the FM state (top panel) as well as the HSS magnetic states (bottom panel). In both cases, the metallic nature of Fe_3Ga_4 is confirmed, and the HSS state shows the presence of a noticeable pseudo-gap effect at the Fermi level.

spin spiral order in the HSS phase of Fe₃Ga₄, temperature and field-dependent neutron diffraction would be required and this work would be integral in identifying the temperature and field regime in which the TCS is stabilized to investigate the universality of the proposed mechanism for the THE in this system. [15].

4. Conclusions

Systematic magnetic and electrical transport measurements were performed on oriented single crystal of Fe₃Ga₄ in order to determine the nature of the magnetic ordering in the intermediate HSS phase. We identify the helical spin spiral order of the AFM state, resolve the metamagnetic transitions within the helical spin spiral state that evolve with temperature and field, describe the unique associated spin configurations, and show through resistivity measurements and theoretical modeling that the AFM state is a metallic HSS. We thus unveil the complex evolution of magnetization with applied field throughout the magnetic phase diagram. We observe behavior that is consistent with the presence of a spin spiral HSS order within the ab-plane, although such behavior has been demonstrated more rigorously in other systems [27]. Notably, no anomalous features in electrical transport measurements was observed near the HSS-FM₂ transition and no **q**-dependent peak was observed in generalized susceptibility at the Fermi level. We take these observations as evidence that the stabilization of the HSS phase in this system is likely driven not solely electronically, but also involves complex interactions of both itinerant and localized electrons in the monoclinic unit cell.

Although the transition to the intermediate phase is not fully understood, the HSS phase is metallic, and it has been shown to exhibit metamagnetic transitions, and to be stable over a wide temperature range, including room temperature [12,24]. This is in stark contrast to the small number of d-electron materials with HSS ordering that manifest at low temperatures and in most cases arise from the Dzyaloshinskii-Moriya interaction and lack of inversion symmetry [31-33]. The centrosymmetric *d*-electron systems that exhibit helical-spin-spiral order has sparked an interest in revisiting theoretical avenues for stabilization of this ordering through exchange interactions, electronic instabilities, and/or quantum fluctuations [34–37]. Additional work is needed to identify the physics driving the HSS phase as well as the metamagnetic transitions through temperature- and field-dependent neutron and polarized neutron diffraction measurements. Furthermore, Hall effect measurements need to be performed within the temperature and field regimes of the HSS phase in order to support the description for the generation of a non-zero topological field through the interaction of the metamagnetic phases and external field. Our study indicates that Fe₃Ga₄ would provide and interesting materials platform for exploring novel magnetic phases arising from complex magnetic interactions as well as the mechanisms giving rise to the THE-like transport signature.

Author Contributions

B.W. and M.E.J. grew the samples and conceptualized the work. X.Z., D.Y.C., and M.G.K. performed single crystal X-ray diffraction. A.F., D.H., V.S, O.B., R.B., and S.P.B performed magnetometry measurements. D.R.B, O.N.M, V.D.B., V.V.S, B.B., A.B. performed theoretical calculations. G.M.S. and A.L.F. performed electrical transport measurements. M.E.J. supervised the project. B.W. and M.E.J. wrote the manuscript with input from all authors. All authors reviewed the results and approved the final version of the manuscript.

Data Availability

All relevant data are available from the authors upon reasonable request.

Declaration of Competing Interest

The authors declare that they have no known competing financial interests or personal relationships that could have appeared to influence the work reported in this paper.

Acknowledgements

Research at the United States Naval Academy was supported by the NSF DMR-EPM 1904446 and ONR 1400844839. Work at Argonne (structural characterization by single crystal X-ray diffraction) was supported by the U.S. Department of Energy, Office of Science, Basic Energy Sciences, Materials Sciences and Engineering Division. Work at Northeastern University was partially supported by the National Science Foundation (USA) grant DMR-1905662 and the Air Force Office of Scientific Research (USA) award FA9550-20-1-0247 (A.F. and D.H.) and the US Department of Energy (DOE), Office of Science, Basic Energy Sciences Grant No. DE-SC0022216 (A.B.) and benefited from Northeastern University's Advanced Scientific Computation Center and the Discovery Cluster and the National Energy Research Scientific Computing Center through DOE Grant No. DE-AC02-05CH11231. We thank A. Feiguin for useful conversations. The work at LUT university was supported by the Ministry of Education and Culture (Finland). Spin-spiral calculations were supported by the RSF - Russian Science Foundation project No. 22-12-20032 . Calculations of ground state for FM, AFM states and their electronic properties were performed with the support of the Ministry of Science and Higher Education of the Russian Federation within the framework of the Russian State Assignment under contract No. 075-01391-22-00. O.N.M. acknowledges the DFG (German Research Foundation) within CRC/TRR 270, project no. 405553726.

Appendix A. Supporting information

Supplementary data associated with this article can be found in the online version at doi:10.1016/j.jallcom.2022.165532.

References

- [1] T. Jungwirth, X. Marti, P. Wadley, J. Wunderlich, Antiferromagnetic spintronics, Nat. Nanotechnol. 11 (2016) 231–241.
- [2] L. Wollmann, A.K. Nayak, S.S. Parkin, C. Felser, Heusler 4.0: tunable materials, Ann. Rev. Mater. Res. 47 (2017) 247–270.
- [3] S.A. Siddiqui, J. Sklenar, K. Kang, M.J. Gilbert, A. Schleife, N. Mason, A. Hoffmann, Metallic antiferromagnets, J. Appl. Phys. 128 (2020) 040904.
- [4] E. Fawcett, Spin-density-wave antiferromagnetism in chromium, Rev. Mod. Phys. 60 (1988) 209.
- [5] Y. Feng, D. Silevitch, J. Wang, A. Palmer, N. Woo, J.-Q. Yan, Z. Islam, A. Suslov, P. Littlewood, T. Rosenbaum, Evolution of incommensurate spin order with magnetic field and temperature in the itinerant antiferromagnet GdSi, Phys. Rev. B 88 (2013) 134404.
- [6] V. Baltz, A. Manchon, M. Tsoi, T. Moriyama, T. Ono, Y. Tserkovnyak, Antiferromagnetic spintronics, Rev. Mod. Phys. 90 (2018) 015005.
- [7] J. Kouvel, J. Kouvel, Anomalous magnetic moments and transformations in the ordered alloy FeRh, Proceedings of the Seventh Conference on Magnetism and Magnetic Materials, Springer, 1962, pp. 1343–1344.
- [8] S. Maat, J.U. Thiele, E.E. Fullerton, Temperature and field hysteresis of the antiferromagnetic-to-ferromagnetic phase transition in epitaxial FeRh films, Phys. Rev. B 72 (2005) 214432.
- [9] R. Barua, F. Jiménez-Villacorta, L. Lewis, Predicting magnetostructural trends in FeRh-based ternary systems, Appl. Phys. Lett. 103 (2013) 102407.

- [10] M. Loving, R. Barua, C. Le Graët, C. Kinane, D. Heiman, S. Langridge, C. Marrows, L. Lewis, Strain-tuning of the magnetocaloric transition temperature in model FeRh films, J. Phys. D: Appl. Phys. 51 (2017) 024003.
- [11] M. Ibarra, P. Algarabel, Giant volume magnetostriction in the FeRh alloy, Phys. Rev. B 50 (1994) 4196.
- [12] J. Mendez, C. Ekuma, Y. Wu, B. Fulfer, J. Prestigiacomo, W. Shelton, M. Jarrell, J. Moreno, D. Young, P. Adams, Competing magnetic states, disorder, and the magnetic character of Fe₃Ga₄, Phys. Rev. B 91 (2015) 144409.
- [13] Y., Wu, Z., Ning, H., Cao, G., Cao, K. A., Benavides, S., Karna, G. T., McCandless, R., Jin, J. Y., Chan, W., Shelton et al., Spin density wave instability in a ferromagnet, Sci. Rep. 8 (2018) 5225.
- [14] B. Wilfong, V. Sharma, J. Naphy, O. Bishop, S.P. Bennett, J. Prestigiacomo, R. Barua, M.E. Jamer, Altering the magnetic ordering of Fe₃Ga₄ via thermal annealing and hydrostatic pressure, J. Alloy. Compd. (2021) 162421.
- [15] M. Afshar, I.I. Mazin, Spin spiral and topological Hall effect in Fe₃Ga₄, Phys. Rev. B 104 (2021) 094418.
- [16] M. Philippe, B. Malaman, B. Roques, A. Courtois, J. Protas, Structures cristallines des phases Fe₃Ga₄ et Cr₃Ga₄, Acta Crystallogr. Sect. B: Struct. Crystallogr. Cryst. Chem. 31 (1975) 477–482.
- [17] G. Kresse, J. Furthmüller, Efficient iterative schemes for ab initio total-energy calculations using a plane-wave basis set, Phys. Rev. B 54 (1996) 11169–11186.
- [18] G. Kresse, D. Joubert, From ultrasoft pseudopotentials to the projector augmented-wave method, Phys. Rev. B 59 (1999) 1758.
- [19] J. Perdew, K. Burke, M. Ernzerhof, Generalized gradient approximation made simple, Phys. Rev. Lett. 77 (1996) 3865.
- [20] H.J. Monkhorst, J.D. Pack, Special points for Brillouin-zone integrations, Phys. Rev. B 13 (1976) 5188.
- [21] L.M. Sandratskii, Energy band structure calculations for crystals with spiral magnetic structure, Phys. Status Solidi (B) 136 (1986) 167–180.
- [22] H. Al-Kanani, J. Booth, High field transitions in (Fe, T)₃Ga₄ alloys, Phys. B 211 (1995) 90–92.
- [23] N. Kawamiya, K. Adachi, Magnetic and mössbauer studies of metamagnetic Fe₃Ga₄, J. Phys. Soc. Jpn. 55 (1986) 634–640.
- [24] S.S. Samatham, K. Suresh, Weak arrest-like and field-driven first order magnetic phase transitions of itinerant Fe₃Ga₄ revealed by magnetization and magnetoresistance isotherms, J. Magn. Magn. Mater. 422 (2017) 174–180.
- [25] C. Stock, E. Rodriguez, P. Bourges, R. Ewings, H. Cao, S. Chi, J. Rodriguez-Rivera, M. Green, Competing spin density wave, collinear, and helical magnetism in Fe₁₊ ,Te, Phys. Rev. B 95 (2017) 144407.
- [26] E.E. Rodriguez, C. Stock, P. Zajdel, K.L. Krycka, C.F. Majkrzak, P. Zavalij, M.A. Green, Magnetic-crystallographic phase diagram of the superconducting parent compound Fe_{1+ x}Te, Phys. Rev. B 84 (2011) 064403.
 [27] N.J. Ghimire, R.L. Dally, L. Poudel, D.C. Jones, D. Michel, N.T. Magar, M. Bleuel,
- [27] N.J. Ghimire, R.L. Dally, L. Poudel, D.C. Jones, D. Michel, N.T. Magar, M. Bleuel, M.A. McGuire, J.S. Jiang, J.F. Mitchell, et al., Competing magnetic phases and fluctuation-driven scalar spin chirality in the kagome metal YMn₆Sn₆, Sci. Adv. 6 (2020) eabe2680.
- [28] Y. Tokura, S. Seki, Multiferroics with spiral spin orders, Adv. Mater. 22 (2010) 1554–1565.
- [29] K.K. Hung, P.K. Ko, C.-M. Hu, Y.C. Cheng, Random telegraph noise of deep-sub-micrometer mosfet's, IEEE Electron Device Lett. 11 (1990) 90–92.
- [30] C. Parman, N. Israeloff, J. Kakalios, Random telegraph-switching noise in coplanar current measurements of amorphous silicon, Phys. Rev. B 44 (1991) 8391.
- [31] S. Mühlbauer, B. Binz, F. Jonietz, C. Pfleiderer, A. Rosch, A. Neubauer, R. Georgii, P. Böni, Skyrmion lattice in a chiral magnet, Science 323 (2009) 915–919.
- [32] N. Ghimire, M.A. McGuire, D.S. Parker, B. Sipos, S. Tang, J.-Q. Yan, B.C. Sales, D. Mandrus, Magnetic phase transition in single crystals of the chiral helimagnet Cr_{1/3}NbS₂, Phys. Rev. B 87 (2013) 104403.
- [33] Y. Togawa, T. Koyama, K. Takayanagi, S. Mori, Y. Kousaka, J. Akimitsu, S. Nishihara, K. Inoue, A. Ovchinnikov, J.-I. Kishine, Chiral magnetic soliton lattice on a chiral helimagnet, Phys. Rev. Lett. 108 (2012) 107202.
- [34] Z. Li, Z. Li, Z. Liu, Y. Xu, Y. Song, D. Huang, N. Shen, A. Ma, S. Li, M. Chi, Frontzek, Flat-band magnetism and helical magnetic order in Ni-doped SrCo₂As₂, Phys. Rev. B 100 (2019) 094446.
- [35] G. Conduit, A. Green, B. Simons, Inhomogeneous phase formation on the border of itinerant ferromagnetism, Phys. Rev. Lett. 103 (2009) 207201.
- [36] J.M. Wilde, A. Kreyssig, D. Vaknin, N.S. Sangeetha, B. Li, W. Tian, P.P. Orth, D.C. Johnston, B.G. Ueland, R.J. McQueeney, Helical magnetic ordering in Sr(Co_{1-x}Ni_x)₂As₂, Phys. Rev. B 100 (2019) 161113.
- [37] N.S. Sangeetha, L.-L. Wang, A.V. Smirnov, V. Smetana, A.-V. Mudring, D.D. Johnson, M.A. Tanatar, R. Prozorov, D.C. Johnston, Non-fermi-liquid types of behavior associated with a magnetic quantum critical point in Sr(Co_{1-x}Ni_x)₂As₂ single crystals, Phys. Rev. B 100 (2019) 094447.